Inorganic Chemistry

pubs.acs.org/IC Article

# Maloplatin-B, a Cisplatin-Based BODIPY-Tagged Mito-Specific "Chemo-PDT" Agent Active in Red Light

Vanitha Ramu, Paramita Kundu, Paturu Kondaiah,* and Akhil R. Chakravarty*

Cite This: *Inorg. Chem.* 2021, 60, 6410−6420 Read Online

ACCESS | Metrics & More | Article Recommendations | Supporting Information

**ABSTRACT:** Maloplatin-B, a cisplatin-based complex, namely $[Pt(\mathbf{A\text{-}BOD})(NH_3)_2](NO_3)$ (**Pt-A-BOD**) with a pendant boron-dipyrromethene (BODIPY) moiety, where **HA-BOD** is a methyl malonyl chloride derived monostyryl BODIPY ligand, was designed and developed as near-IR light (600−720 nm) organelle-targeting photodynamic therapy agent. The complex $[Pt(acac)(NH_3)_2](NO_3)$ (**Pt-Ac**) was used as a control. **Pt-A-BOD** displayed an absorption band at 616 nm ($\varepsilon = 2.9 \times 10^4$ $M^{-1}$ $cm^{-1}$) in 10% dimethyl sulfoxide/Dulbecco's Modified Eagle's Medium (DMSO/DMEM, pH 7.2). This complex displayed a broad emission band within 650−850 nm with a $\lambda_{em}$ value of 720 nm in 10% DMSO−DMEM (pH 7.2) upon excitation ($\lambda_{ex}$) at 615 nm with a large Stokes shift. The fluorescence quantum yield ($\Phi_F$) value for **Pt-A-BOD** is 0.032 and for the ligand **HA-BOD** is 0.24. The BODIPY complex and ligand showed the formation of singlet oxygen as the ROS (reactive oxygen species) on irradiation with near-IR red light of 660 nm, as evidenced from a 1,3-diphenylisobenzofuran (DPBF) assay. The complex displayed remarkable apoptotic NIR light-induced PDT activity with half-maximum inhibitory concentration values ($IC_{50}$) of 1.6−2.4 $\mu$M in A549 lung and HeLa cervical cancer cells, while it was less active in the dark. The cellular ROS generation by the complex in red light was ascertained by a DCFDA (2′,7′-dichlorofluorescein diacetate) assay. Cellular imaging showed its localization primarily in the mitochondria of A549 cancer cells. The JC1 and Annexin-V FITC/PI assays carried out for A549 cancer cells treated with the BODIPY complex showed the alteration of mitochondrial membrane potential and apoptotic cell death on near-IR red light (600−720 nm) irradiation, respectively.

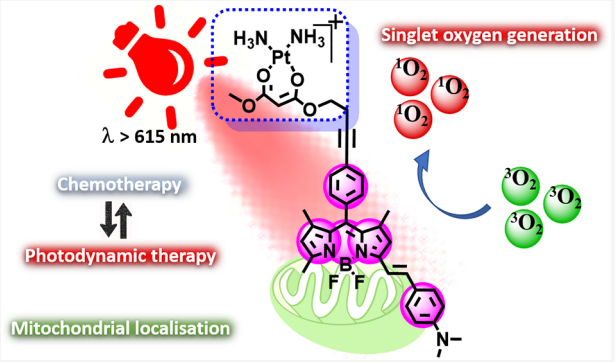




## INTRODUCTION

The serendipitous discovery of cisplatin (CP) has led to the foundation of the chemistry of metal-based anticancer agents, and this has propelled the later discovery of two other platinum-based drugs: namely, carboplatin and oxaliplatin.[1−4] The impetus to search for new Pt-based drugs originates from the major side effects associated with CP due to rapid intracellular Pt−Cl bond dissociation kinetics thus necessitating the design and synthesis of new CP analogues having the Pt−Cl bond replaced by other ligands, with the complex generating the active platinum species at a slower rate in comparison to CP, thus enhancing the efficacy of the drug.[3,5−8] For example, oxaliplatin and carboplatin having O,O-donor dianionic ligands release the active platinum species at a slower rate in comparison to CP and display better anticancer properties.[5−8] A few other CP analogues such as nedaplatin, heptaplatin, lobaplatin, aroplatin, spiroplatin, enloplatin, zeniplatin, miboplatin, picoplatin, ormaplatin, iproplatin, etc. have been reported to show promising activity to make them suitable for the treatment of cancer.[9−14] In a parallel development, Lippard and co-workers have enriched the chemistry of monofunctional platinum-based drugs, but such drugs showed reduced therapeutic activity in comparison to the bifunctional CP analogues.[15,16]

Subsequently, to address the specificity and efficacy of CP and its analogues, apparently inactive platinum(IV) complexes have been developed and reported by researchers in recent years.[17−19] Two axial ligands in the pseudo-octahedral geometry derived from the CP core have tumor-targeting properties. These complexes are suitable for targeted chemotherapy, where the axial bonds can be released on cellular reduction of Pt(IV) by thiols to Pt(II), thus generating active platinum(II) species. In a different approach, Sadler and co-workers have developed platinum(IV) complexes as prodrug molecules which can generate the active chemotherapeutic drug CP or its analogue on UV light irradiation.[5] Photo-activated chemotherapy (PACT) has been developed as an

Received: January 15, 2021
Published: April 12, 2021

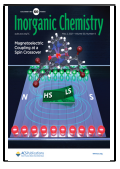




https://doi.org/10.1021/acs.inorgchem.1c00124
*Inorg. Chem.* 2021, 60, 6410−6420

effective modality to selectively activate a drug in the cancer cells by light irradiation while the noncancerous cellular environment is protected.[20−22] A simultaneous development has occurred with the use of transition-metal complexes in the photodynamic therapy (PDT) of cancer.[23−25] PDT was developed before to CP as an alternate therapeutic modality different from chemotherapy and radiation therapy but got FDA (Food and Drug Administration) approval after CP. In the conventional PDT, a photosensitizer, namely Photofrin, in the cancer cell is photoirradiated with red light in the presence of molecular oxygen ($^3O_2$) to generate highly cytotoxic singlet oxygen ($^1O_2$) that kills the photoexposed cancer cells, thus leaving the unexposed healthy cells unaffected.[25−27]

A combination of PDT- and CP-based chemotherapy can be achieved by designing a new generation of cisplatin-derived platinum(II) complexes having a dissociable ligand tagged with a photosensitizer as a "chemo-PDT" agent that can generate singlet oxygen on irradiation using near-IR red light.[28−30] The light within the PDT spectral window has the advantage of the highest penetration to reach the cancer cells in deep tissues for better efficacy, and red-light-absorbing tissue chromophores are generally absent in the human body. Although Photofrin is the FDA-approved PDT drug, it suffers from selectivity, post-treatment skin sensitivity, and hepatotoxicity.[31−34] Reports from our group have shown that boron-dipyrromethene-appended transition-metal complexes can be used as photosensitizers for generating singlet oxygen in high yield on light activation.[35−40] BODIPY dyes have good photostability, and their core is amenable for tuning the absorption and emission properties within a broad spectral window ranging from the visible to the near-IR region.[41,42] In addition, BODIPY dyes can be tuned to localize into different cellular organelles, thus specifically enhancing their therapeutic potential.[43−46] We have recently reported a diplatinum(II) catecholate, [{Pt(dach)}$_2$($\mu$-Dcrb)] (DP), where dach is 1,2-diaminocyclohexane and Dcrb is a tetraanionic morpholine-conjugated BODIPY-linked dicatecholate base, as a lysosome-targeting PDT agent in red light.[47] This complex acts more as an organelle-targeting PDT agent localizing in lysosomes than as a chemotherapeutic agent with $IC_{50}$ values of 0.6 $\mu$M in HeLa cells in red light (600−720 nm) and 105 $\mu$M in the dark with a remarkable PI (phototoxic index) value. The present work stems from our interest in improving the model by using $\{Pt(NH_3)_2\}^{2+}$ of CP bonded to an O,O-donor chelating ligand having an appended red-light-active BODIPY moiety. The O,O-donor ligand derived from the methyl malonyl chloride (methyl chloroformylacetate) framework is a suitable replacement for oxalic or dicarboxylic acid in comparison to aromatic catecholate base.[48] Herein, we present a platinum(II) complex, [Pt(**A-BOD**)$(NH_3)_2$]$(NO_3)$ (**Pt-A-BOD**), having a red-light-activatable BODIPY ligand that could release an active platinum(II) species for chemotherapeutic action while it initiates PDT activity involving the monostyryl BODIPY unit in red light (Figure 1). The complex **Pt-A-BOD** as a "chemo-PDT" agent has a cisplatin-like backbone structure with a chelating methyl malonate tagged to a monostyryl BODIPY. The use of a malonyl-based O,O-donor ligand in a platinum complex is to ensure slow release of the active platinum species $\{Pt(NH_3)_2\}^{2+}$ that can possibly bind to DNA (nuclear and/or mitochondrial) and act as a transcription inhibitor. Significant results of this study include high PDT activity of the complex in red light, giving submicromolar $IC_{50}$ values, while being essentially nontoxic in the dark, mitochondrial localization, a high yield of singlet oxygen generation, and apoptotic cellular death promoted by reactive oxygen species (ROS). In addition, the ligand H**A-BOD** alone is significantly less toxic than the complex, justifying the importance of coordination to the heavy metal platinum that is needed to promote facile intersystem crossing (ISC) in a type II process for the activation of molecular oxygen. The complex **Pt-A-BOD**, denoted Maloplatin-B, derived from a cisplatin framework exemplifies a rare chemo-PDT agent due to its dual activity.

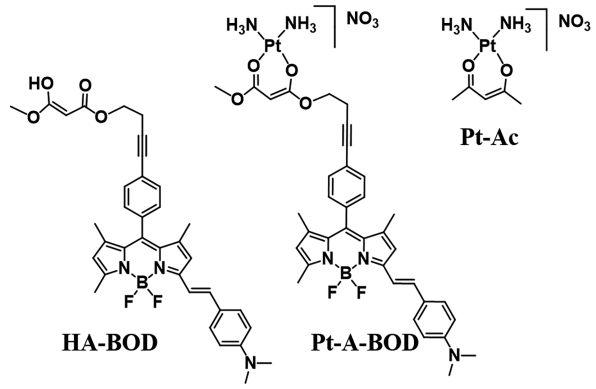


**Figure 1.** Chemical structures of the ligand H**A-BOD**, [Pt(**A-BOD**)$(NH_3)_2$]$(NO_3)$ (**Pt-A-BOD**) as an active platinum(II) complex, and [Pt(acac)$(NH_3)_2$]$(NO_3)$ (**Pt-Ac**) as a control species.

## EXPERIMENTAL SECTION

**Materials and Methods.** All of the chemicals and reagents were obtained from commercial sources (see the Supporting Information). The ligand H**A-BOD** and complexes **Pt-A-BOD** and **Pt-Ac** were prepared by following literature reports with some modifications.[37,48] $^1H$, $^{11}B$, and $^{13}C$ NMR spectra were recorded using a Bruker Avance 400 MHz NMR spectrometer. An Agilent Model 6538 Ultra High Definition Accurate Mass-Q-TOF (LC-HRMS) instrument was used to obtain mass spectral data. A Thermo Finnigan Flash EA 1112 CHNS analyzer was employed for elemental analysis. The platinum complex showed a marginally lower carbon percentage in the elemental analysis possibly due to poor or insufficient combustion of the sample under the standard conditions used. Bruker Alpha and PerkinElmer Spectrum 750 spectrophotometers were used for recording UV−visible spectra. A HORIBA Jobin Yvon IBH TCSPC fluorimeter (fitted with FluoroHub analysis software) was used to record emission spectra. The geometries of the platinum complexes were optimized using the B3LYP/LANL2DZ level of theory. By standard protocols, a red-light photoreactor (Waldmann PDT 1200 L) was used for the red-light experiments. Cytotoxic data were obtained from a TECAN microplate reader by using GraphPad Prism 6 software. Flow cytometry experiments were done using a Becton Dickinson fluorescence-activated cell sorting (BD-FACS) Verse instrument (BD Biosciences). It was configured with a MoFLo XDP cell sorter, three lasers of wavelengths 488, 365, and 640 nm, and 10-color parameters. FACS data acquisition and analysis were done using the Windows 7 operating system and BD-FACS suite software. Confocal microscopy images were obtained from a Zeiss LSM 880 with Airyscan confocal microscope. It had an oil immersion lens with a magnification of 63×. The images were processed by using Zeiss software.

**Synthesis.** Ligand H**A-BOD**, namely 4-(4-(3-((*E*)-4-(dimethylamino)styryl)-5,5-difluoro-1,7,9-trimethyl-5*H*-4l4,5l4-dipyrrolo[1,2-*c*:2′,1′-*f*][1,3,2]diazaborinin-10-yl)phenyl)but-3-yn-1-yl (*E*)-3-hydroxy-3-methoxyacrylate, and the platinum complexes, namely **Pt-A-BOD** and **Pt-Ac**, were synthesized by following the literature procedures.[37,48,49] The steps involved in the synthesis of the ligand H**A-BOD** and the complexes are provided as Schemes S1 and S2 in the Supporting Information. The detailed procedures employed


https://doi.org/10.1021/acs.inorgchem.1c00124
Inorg. Chem. 2021, 60, 6410−6420

in the synthesis of the ligand and the complexes along with the characterization data are given below.

**HA-BOD.** The precursor BODIPY compound mBOD-OL, namely 4-(4-(3-(4-(dimethylamino)styryl)-5,5-difluoro-1,7,9-trimethyldipyrrolo[1,3,2]diazaborinin-10-yl)phenyl)but-3-yn-1-ol (212 mg, 0.5 mmol, 1 equiv), was dissolved in 10 mL of freshly distilled dichloromethane. Under an $N_2$ atmosphere, pyridine (11 mg, 0.14 mmol) was added. After the resulting mixture was cooled in an ice bath for 15 min, methyl malonyl chloride (17 mg, 0.13 mmol) in 5 mL of distilled dichloromethane was added dropwise. The resulting mixture was further warmed to room temperature followed by continuous stirring for 12 h. The reaction mixture was filtered and extracted with dichloromethane. It was concentrated using a rotavap, and the product was isolated by silica gel column chromatography using dichloromethane/hexane as eluent in the ratio of 65/35 (v/v).

Blue solid (158 mg). Yield: ∼54%. Anal. Calcd for $C_{36}H_{36}BF_2N_3O_4$ ($M_w$: 623.508): C, 69.35; H, 5.82; N, 6.74. Found: C, 68.92; H, 5.50; N, 6.68. ESI-MS $m/z$: calcd, 624.2749; found $[M + H]^+$, 624.2849. $^1$H NMR (400 MHz, DMSO-$d_6$): $\delta$ (ppm) 7.57 (s, 2 H), 7.53 (s, 2 H), 7.32 (s, 1 H), 7.28 (s, 1 H), 7.24 (s, 1 H), 7.12 (s, 1 H), 6.72 (s, 1 H), 6.70 (s, 1 H), 6.62 (s, 1 H), 5.99 (s, 1 H), 5.04 (s, 1 H), 4.40 (t, 2 H, 4 Hz), 3.63 (s, 3 H), 3.05 (s, 6 H), 2.85 (t, 2 H, 4 Hz), 1.47 (s, 3 H), 1.44 (s, 6H) (s, singlet; d, doublet; t, triplet). $^{13}$C NMR (100 MHz, DMSO-$d_6$): $\delta$ (ppm) 152.38, 139.73, 138.55, 135.67, 138.27, 132.71, 129.04, 125.07, 124.32, 123.95, 118.33, 116.35, 114.74, 112.48, 63.70, 53.04, 41.71, 35.19, 34.30, 32.10, 29.40, 23.16, 20.30, 15.06, 14.61. UV−vis (10% DMSO/DMEM at pH 7.2): $\lambda_{max}$, nm ($\varepsilon$, $M^{-1}$ $cm^{-1}$) 614 ($4.4 \times 10^4$). Emission spectrum (10% DMSO/DPBS at pH 7.2): $\lambda_{em}$ ($\lambda_{ex}$, $\Phi_F$) 720 nm (615 nm, 0.24).

**[Pt(A-BOD)(NH$_3$)$_2$](NO$_3$), (Pt-A-BOD).** cis-[Pt(NH$_3$)$_2$Cl$_2$] (cisplatin, 190 mg, 0.5 mmol, 1 equiv) was treated with $AgNO_3$ (162 mg, 0.98 mmol) in 5 mL of distilled water and stirred at room temperature for 24 h in the dark and then filtered twice to remove AgCl. The yellowish filtrate was added to a solution of the ligand **HA-BOD** (165.5 mg, 0.25 mmol, 1 equiv) and 1 mL of freshly distilled triethylamine in a dropwise manner and stirred for 4 h in the dark at room temperature in methanol (30 mL). Using a rotavap the methanol solvent was removed and the solid was dissolved in DMF (2 mL). The desired complex was precipitated by adding excess diethyl ether. To eliminate any unreacted starting materials, the precipitated complex was repetitively treated with water and diethyl ether to obtain the pure product.

Dark blue solid (172 mg). Yield: ∼54%. Anal. Calcd for $C_{36}H_{41}BF_2N_6O_7Pt$ ($M_w$: 914.657): C, 47.27; H, 4.63; N, 9.29. Found: C, 45.29, H, 4.44; N, 9.50. ESI-MS $m/z$: calcd, 852.2900; found, 852.2616 $[M - NO_3]^+$. $^1$H NMR (400 MHz, DMSO-$d_6$): $\delta$ (ppm) 7.56 (s, 2 H), 7.49 (s, 1 H), 7.45 (s, 2 H), 7.37 (s, 1 H), 7.36 (s, 2 H), 7.24 (s, 1 H), 7.20 (s, 1 H), 6.91 (s, 1 H), 6.12 (s, 1 H), 5.30 (s, 1 H), 4.76 (s, 3 H), 4.66 (s, 3 H), 4.26 (s, 2 H), 3.16 (s, 3 H), 2.98 (s, 6 H), 2.81 (s, 2 H), 1.40 (s, 3H), 1.33 (s, 6 H). $^{13}$C NMR (100 MHz, DMSO-$d_6$): $\delta$ (ppm) 167.43, 167.01, 143.18, 138.25, 132.56, 129.52, 129.15, 123.95, 123.85, 118.89, 112.98, 112.60, 63.22, 52.65, 46.24, 41.37, 31.70, 29.39, 22.52, 14.86, 14.39, 9.03. UV−vis (10% DMSO/DMEM at pH 7.2): $\lambda_{max}$, nm ($\varepsilon$, $M^{-1}$ $cm^{-1}$) 616 ($2.9 \times 10^4$). Emission spectrum (10% DMSO/DPBS at pH 7.2): $\lambda_{em}$ ($\lambda_{ex}$, $\Phi_F$) 720 nm (615 nm, 0.032). $\Lambda_M$ in DMF: 76 S $m^2$ $mol^{-1}$.

**Cellular Experiments.** HeLa (human cervical cancer cell line), A549 (human lung adenocarcinoma cell line), and HPL1D (immortalized human lung epithelial cell line) were cultured in Dulbecco's modified Eagle's medium (DMEM) supplemented with 10% fetal bovine serum (FBS) under a 5% $CO_2$ atmosphere at 37 °C. A 3-(4,5-dimethylthiazol-2-yl)-2,5-diphenyltetrazolium bromide (MTT) assay was carried out to determine the photocytotoxicities of the complexes in red light. Approximately 8000 cells of HeLa, A549, and HPL1D were plated separately in two different 96-well culture plates. After ∼24 h, the cells were treated with various concentrations of the compounds, namely **HA-BOD**, **Pt-A-BOD**, and **Pt-Ac**, from 0.195 to 100 $\mu$M in 1% DMSO/DMEM and the cells were further incubated for 4 h under a 5% $CO_2$ atmosphere at 37 °C in the dark. The DMEM-buffer-containing compounds were removed in one set of the cells and washed with DPBS buffer, and the cells were then subjected to red-light irradiation for 15 min ($\lambda$ = 600−720 nm, light dose 30 $J$ $cm^{-2}$, Waldmann PDT 1200 L). Meanwhile, the DMEM-buffer-containing compounds were replaced with fresh DMEM from the other set of cells. After irradiation the PBS buffer was replaced with fresh DMEM in the irradiated cells and both sets of cells were further incubated for 16 h in dark. Data were obtained by carrying out experiments with three independent sets. For each concentration, the experiment was done in triplicate and the $IC_{50}$ (half maximum inhibitory concentration) values were obtained by using Graph Pad Prism 6 and employing a nonlinear regression analysis. The DNA binding experiments were performed in Tris-HCl buffer (5 mM, pH 7.2) using a DMF solution of the complex and calf thymus DNA (complete experimental details are provided in the Supporting Information).

For the confocal laser scanning microscopy (CLSM) experiments, A549 cells were cultured in Dulbecco's modified Eagle's medium supplemented with 10% FBS under a 5% $CO_2$ atmosphere at 37 °C. Approximately $1 \times 10^5$ cells were seeded onto 35 mm round glass bottom dishes. After 24 h, A549 cells were incubated with the compounds **HA-BOD** and **Pt-A-BOD** (2 $\mu$M) in 1% DMSO/DMEM for 4 h. Before imaging, the cells were washed with DPBS and were treated with Mitotracker Green (MTG, 200 nM, 15 min) and 4′,6-diamidino-2-phenylindole (DAPI) as respective mitochondria- and nucleus-selective trackers. The CLSM images were recorded in fresh DMEM by maintaining a 5% $CO_2$ atmosphere at 37 °C in the dark by using a Zeiss LSM 880 with Airyscan microscope with an oil immersion lens having a magnification of 63×. For the cells incubated with the compounds **HA-BOD** and **Pt-A-BOD**, the CLSM images were captured with a band path of 650−750 nm upon excitation at 633 nm. The fluorescence of Mito Tracker Green in A549 cells was captured with a band path of 520−560 nm upon excitation at 508 nm, and for DAPI, the emission detection band path was set to 420−460 nm with an excitation of 408 nm. To confirm the results, multiple CLSM images were obtained and the experiments were carried out in duplicate.

For the detection of singlet oxygen generation inside the cells, the cells were treated with **Pt-A-BOD** (2 $\mu$M) in 1% DMSO/DMEM for 4 h. Further, the cells were rinsed with DPBS and were incubated with singlet oxygen sensor green (SOSG) (10 $\mu$M, 30 min), washed with DPBS before red-light irradiation ($\lambda$ = 600−720 nm, light dose 30 $J$ $cm^{-2}$) for the light case and subjected to CLSM for the dark set of cells. For the determination of mitochondrial membrane potential disruption in A549 cells, the cells were treated with **Pt-A-BOD** (2 $\mu$M) in 1% DMSO/DMEM for 4 h. Further, the cells were rinsed with DPBS, incubated with JC1 (5,5,6,6′-tetrachloro-1,1′,3,3′-tetraethylbenzimidazoylcarbocyanine iodide) dye (100 $\mu$M, 4 h), washed with DPBS before red-light irradiation ($\lambda$ = 600−720 nm, light dose 30 $J$ $cm^{-2}$ in the case of light), and subjected to CLSM for the dark set of cells. For an analysis of the extent of bleaching of the complex **Pt-A-BOD** in A549 cells, the cells were treated with **Pt-A-BOD** (2 $\mu$M) in 1% DMSO/DMEM for 4 h and subjected to CLSM to record images at time intervals of 30 s for 20 min. The live cellular uptake of the complex **Pt-A-BOD** (1 $\mu$M) in 1% DMSO/DMEM was determined under a 5% $CO_2$ atmosphere at 37 °C in the dark.

The flow cytometry analysis experiments were performed with approximately $2 \times 10^5$ A549 cells seeded in six-well plates using DMEM supplemented with 10% FBS maintained under a 5% $CO_2$ atmosphere at 37 °C. The generation of reactive oxygen species (ROS) inside A549 cells was detected by a 2′,7′-dichlorofluorescein diacetate (DCFDA) assay. A549 cells were treated with the compounds **Pt-A-BOD** and **HA-BOD** (2 $\mu$M) in 1% DMSO/DMEM for 4 h in the dark. After incubation, the medium was removed, the cells were harvested by trypsinization, and a single cell suspension was prepared. The cells were subsequently treated with 1 $\mu$M DCFDA (solution prepared with DMSO) in the dark for 10 min at room temperature. The distribution of DCFDA-stained A549 cells was obtained by flow cytometry in the FL-1 channel by a BD-FACS Verse instrument. Cellular uptake experiments were carried out for the fluorescent compounds **Pt-A-BOD** and **HA-BOD** (2 $\mu$M) in 1%


https://doi.org/10.1021/acs.inorgchem.1c00124
Inorg. Chem. 2021, 60, 6410−6420

DMSO/DMEM in A549 cells. The distribution of the compounds in stained cells was observed in the APC channel. The mode of cell death induced by the compounds in A549 cells was determined by an AnnexinV-FITC (fluorescein isothiocyanate) experiment. Two sets of cells were treated with both compounds (2 $\mu$M) in 1% DMSO/DMEM for 4 h. One of the plates was exposed to red-light photoirradiation ($\lambda$ = 600−720 nm, light dose 30 $J$ cm$^{-2}$) in DPBS with subsequent addition of fresh media. The cells were further incubated for 19 h, trypsinized, and washed twice with DPBS. The cells were resuspended in 400 $\mu$L of 1X binding buffer, and 1.0 $\mu$L of Annexin V-FITC and 1.0 $\mu$L of PI (propidium iodide) were added to each cell suspension. These tubes were then incubated at room temperature for 10 min in the dark and were further subjected to a FACS analysis.

## RESULTS AND DISCUSSION

**Synthesis and General Properties.** The ligand H**A-BOD** and its platinum(II) complex [Pt(**A-BOD**) $(NH_3)_2$](NO$_3$) (**Pt-A-BOD**), as a cisplatin analogue, were synthesized as stable species in moderate yields. The compounds were characterized with NMR and mass spectral data (Figures S1−S8 in the Supporting Information). The purity of the compounds was ascertained from the $^1$H NMR spectral and elemental analysis data. The complex **Pt-A-BOD** displayed a peak in the mass spectrum at $m/z$ 852.2616 in methanol along with the characteristic isotopic distribution of platinum (Figure S2 in the Supporting Information). The $^1$H NMR spectra of the complex **Pt-A-BOD** and ligand H**A-BOD** displayed peaks characteristic of monosubstituted styryl BODIPY (Figures S3 and S4 in the Supporting Information). The characteristic peaks for the ammine protons were observed in the $^1$H NMR spectra of the complex **Pt-A-BOD** within the range 4.6−4.8 ppm, and the aromatic protons were shifted downfield from 6.6−7.6 ppm to 6.9−7.6 ppm, which indicated the formation of the platinum(II) complex. The $^{13}$C NMR spectra of both the complex and ligand showed peaks corresponding to the carbon atoms in the monosubstituted styryl BODIPY (Figures S5 and S6 in the Supporting Information). The $^{11}$B NMR spectra of both the complex and ligand displayed respective characteristic triplet peaks at 0.84 and 0.927 ppm corresponding to a $BF_2$ unit in a monosubstituted styryl boron-dipyrromethene (BODIPY) moiety (Figures S7 and S8 in the Supporting Information). The solution conductivity measurements gave a molar conductivity value of ∼76 S m$^2$ M$^{-1}$ in dimethylformamide, suggesting a 1/1 electrolytic behavior of the complex. Both the complex and ligand are fairly soluble in solvents such as as chloroform, dichloromethane, methanol, dimethylformamide (DMF), and dimethyl sulfoxide (DMSO).

The UV−visible spectroscopic study was done in pH 7.2 10% DMSO/DMEM buffer (v/v). H**A-BOD** and **Pt-A-BOD** displayed absorption bands at 614 nm ($\varepsilon$ = 4.4 × 10$^4$ M$^{-1}$ cm$^{-1}$) and 617 nm ($\varepsilon$ = 2.9 × 10$^4$ M$^{-1}$ cm$^{-1}$), respectively (Figure 2a). The lowest energy absorption bands were assigned to electronic transitions involving a monostyryl BODIPY unit having a dimethylamino group; the attachment of two 4-(dimethylamino)phenylethynyl moieties results in the shift in the absorption and emission bands toward the red region from the core BODIPY. The UV−visible absorption spectrum of **Pt-A-BOD** was recorded in methanol and acetonitrile solvents, and the extent of the shift was analogous with that observed for 4-(dimethylamino)phenylethynyl BODIPY analogues (Figures S9 and S10 in the Supporting Information). The broadening of the absorption spectra of **Pt-A-BOD** in more polar solvents was observed, suggesting a weak charge transfer character (Figure S9 in the Supporting Information). Such high values of the absorption coefficients for the absorption bands within the PDT spectral window are conducive for a desirable photosensitizing effect. The presence of platinum as a heavy metal in **Pt-A-BOD** makes this complex suitable as a photosensitizer for PDT activity. The control complex **Pt-Ac**, lacking any visible band, is not a PDT-active species. Both **Pt-A-BOD** and H**A-BOD** upon excitation at 615 nm displayed a broad emission band within 650−850 nm with a maximum at 720 nm in pH 7.2 10% DMSO−DMEM (Figure 2b). A partial charge transfer effect, observed in BODIPY moieties having dimethylamino groups as styryl units, resulted in large Stokes shifts in the emission spectra of **Pt-A-BOD** and H**A-BOD**. The complex **Pt-A-BOD** gave a fluorescence quantum yield ($\Phi_F$) value of 0.032. This is much lower in comparison to the $\Phi_F$ value of the ligand ($\Phi_F$ = 0.24). This reduction is attributed to the presence of platinum(II) bonded to the ligand facilitating ISC. The ligand and complex both generated singlet oxygen under red-light irradiation with a singlet oxygen quantum yield ($\Phi_\Delta$) value of 0.19 for the ligand and 0.48 for the complex. Time- and temperature-dependent UV−visible measurements were also done to ascertain the stability of the BODIPY complex and its ligand in 10% DMSO/DMEM, 1% DMSO/DMEM, and also DMSO alone for a time period of up to 48 h in dark. The temperature-dependent UV−visible absorption spectra of **Pt-A-BOD** kept at 4 and 37 °C for 4 h displayed no significant change in absorbance from that kept at room temperature. The results displayed a very negligible decrease in the absorbance of **Pt-A-BOD** in 10% DMSO/DMEM and DMSO, but a small decrease was observed in 1% DMSO/DMEM (Figure S10 in the Supporting Information). Both the complex and ligand were thus found to be stable.

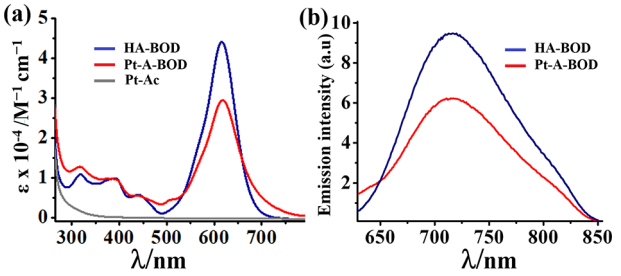


**Figure 2.** (a) Electronic absorption and (b) emission ($\lambda_{ex}$ = 615 nm) spectra of the complexes **Pt-Ac** (nonemissive) and **Pt-A-BOD** and the ligand H**A-BOD** in 10% DMSO−DMEM (pH 7.2).

The energy -optimized structure of the complex **Pt-A-BOD** was obtained by density functional theory (DFT) by using the B3LYP/LANL2DZ level of theory (Figure 3 and Tables S1 and S2 in the Supporting Information).[50,51] For the atoms, the electronic charge density distributions pertaining to the frontier molecular orbitals were obtained through DFT. The energy-minimized structure of **Pt-A-BOD** showed a square-planar geometry with platinum(II) bonded to two ammine groups in a cis disposition and the O,O-donor methyl malonate moiety of the monoanionic **A-BOD** ligand bonded to the metal in a chelating mode. The HOMO (highest occupied molecular orbital) and LUMO (lowest unoccupied molecular orbital) are shown in Figure 3. The HOMO of the complex **Pt-A-BOD** was found to be on the BODIPY-appended methyl malonate unit, while the LUMO was


https://doi.org/10.1021/acs.inorgchem.1c00124
Inorg. Chem. 2021, 60, 6410−6420

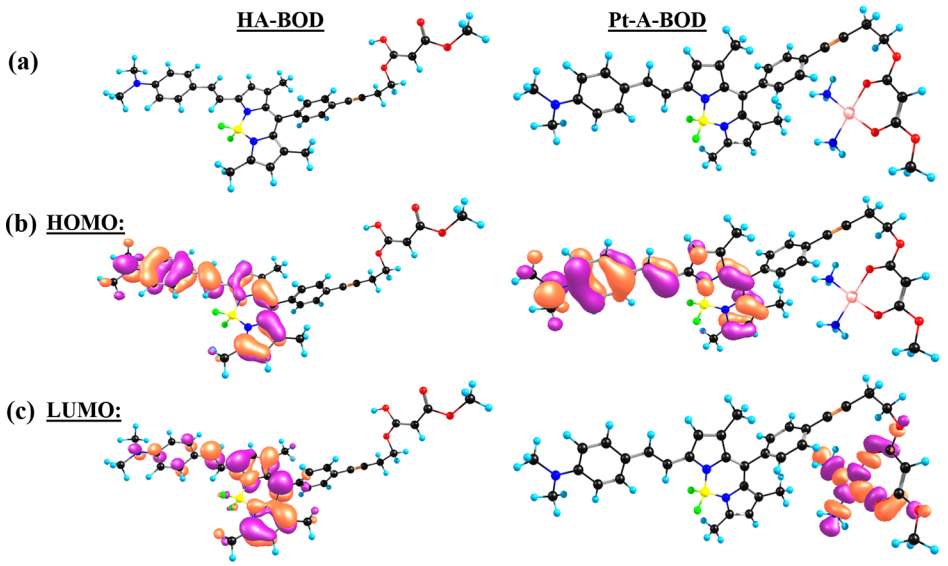


**Figure 3.** Energy-minimized structure (a) and the FMOs, namely the HOMO (b) and LUMO (c), of the ligand **HA-BOD** and complex **Pt-A-BOD** using density functional theory.

localized on the Pt−O bonds. Both the HOMO and LUMO of the ligand **HA-BOD** were localized on monostyryl BODIPY. The DFT data were useful toward an understanding of the spectral properties of the compounds.

**Photocytotoxicity in Red Light.** The complex **Pt-A-BOD**, ligand **HA-BOD**, and control **Pt-Ac** were studied by an MTT assay for their photoinduced cytotoxicity in red light (600−720 nm) with a 4 h preincubation of the compounds in lung cancer cells (A549), an immortalized lung epithelial cell line (HPL1D), and human cervical cancer cells (HeLa) followed by 20 h postincubation. The results of the MTT assay in the form of $IC_{50}$ values are given in Table 1 (Figures S11 and S12 in the Supporting Information). The values for the complex **Pt-Ac** in red light ($\lambda$ = 600−720 nm, light dose 30 $J$ cm$^{-2}$) and in the dark for an incubation time of 24 h were above 100 $\mu$M in these cells. In contrast, the same complex displayed noticeable dark toxicity with an $IC_{50}$ value of 72 $\mu$M for 24 h of incubation in A549 cells, indicating its chemotherapeutic action due to the presence of the platinum-(II) center (Figure S11 in the Supporting Information). The complex **Pt-A-BOD** having a monostyryl BODIPY moiety displayed remarkable near-IR light ($\lambda$ = 600−720 nm, light dose 30 $J$ cm$^{-2}$) photocytotoxicity with $IC_{50}$ values of 1.6−2.4 $\mu$M in the cancer cells with low dark cytotoxicity ($IC_{50}$ = 79−85 $\mu$M). The ligand **HA-BOD** in comparison showed low cytotoxicity in the cancer cells in red light ($\lambda$ = 600−720 nm, light dose 30 $J$ cm$^{-2}$), giving $IC_{50}$ values within 40−52 $\mu$M, possibly due to lower singlet oxygen production. The chemotherapeutic activity of the complex **Pt-A-BOD**, assumed to be occurring due to the presence of the active "cisplatin" unit, was determined from an MTT assay, and the $IC_{50}$ value was 44 $\mu$M for 24 h of incubation with the complex. The $IC_{50}$ value of the ligand **HA-BOD** was >100 $\mu$M for 24 h incubation in the dark. The possibility of any interaction of the complex **Pt-A-BOD** with DNA was studied by UV−visible absorption spectral studies using calf thymus (ct) DNA. The ct-DNA binding constant ($K_b$) for **Pt-A-BOD** was found to be ∼3.9 × 10$^6$ M$^{-1}$ in 5% DMF-Tris buffer (pH 7.2), implying that the complex interacts with DNA through groove binding and/or an intercalative mode (Figure S13 in the Supporting Information).[52] The results indicate the utility of platinum in **Pt-A-BOD** for singlet oxygen generation and the remarkable PDT effect along with a DNA binding interaction with the possibility of inducing a chemotherapeutic effect. The complex **Pt-A-BOD** and ligand **HA-BOD** both showed lower cytotoxicity in immortalized human lung epithelial HPL1D cells in the dark and with light (red light, $\lambda$ = 600−720 nm, light dose 30 $J$ cm$^{-2}$).

**Table 1. MTT Assay Data ($IC_{50}$/$\mu$M) of the Complexes Pt-Ac and Pt-A-BOD and the Ligand HA-BOD**

| cell line | conditions | Pt-Ac | Pt-A-BOD | HA-BOD |
|---|---|---|---|---|
| HeLa | L[a] | >100 | 2.4 ± 0.2 | 40.0 ± 0.2 |
| | D[b] | >100 | 79.0 ± 3.2 | 102.0 ± 3.2 |
| A549 | L[a] | >100 | 1.6 ± 0.2 | 52.0 ± 0.2 |
| | D[b] | >100 | 85.0 ± 0.4 | 97.0 ± 0.4 |
| | D[c] | 72.0 ± 0.2 | 44.0 ± 0.4 | >100 |
| HPL1D | L[a] | 92.1 ± 1.1 | 33.4 ± 0.4 | 63.0 ± 0.6 |
| | D[b] | >100 | 101.0 ± 1.2 | >100 |

[a]$IC_{50}$ values are in $\mu$M with 4 h preincubation in dark with subsequent to red light exposure (L, 600−720 nm, light dose of 30 $J$ cm$^{-2}$ using Waldmann PDT 1200 L). Post incubation period was of 19 h. [b]$IC_{50}$ values are in $\mu$M for samples in the dark. [c]On 24 h incubation under dark.

**Cellular Uptake.** The mode of cellular uptake and the time-dependent cellular internalization ability of a drug being of importance, the time-dependent cellular uptake of the complex was analyzed from a fluorescence-activated cell sorting (FACS) analysis in A549 cells. The cells were incubated with the fluorescent compounds **Pt-A-BOD** and **HA-BOD** (2 $\mu$M) for different time periods of incubation: namely, 2, 4, and 6 h. The cellular fluorescence of the complex and ligand was detected through the APC channel ($\lambda_{ex}$ = 633 nm). There was a large shift in the histogram of both types of treated cells in comparison to the histogram of untreated cells, clearly indicating the cellular uptake of these compounds. For the complex **Pt-A-BOD**, the fluorescence slightly increased as the time of incubation increased from 2 to 4 h but there was no significant difference in the fluorescence emission between 4


https://doi.org/10.1021/acs.inorgchem.1c00124
Inorg. Chem. 2021, 60, 6410−6420

and 6 h (Figure 4a). This indicated the maximum uptake of **Pt-A-BOD** (2 $\mu$M) at 2 h. However, for the ligand, the fluorescence gradually increased with increasing time from 2 to 6 h. To determine the uptake pathway, A549 cells were treated with the complex and ligand (2 $\mu$M) in 1% DMSO/DMEM at the two temperatures 37 and 4 °C. The compounds were incubated for two time periods of 2 and 4 h and subjected to confocal laser scanning microscopy (CLSM) following standard protocols. Cells treated with both the complex and ligand showed almost no fluorescence emission, indicating no apparent cellular uptake on incubation at 4 °C, whereas fluorescence emission was observed on incubation at 37 °C. The results suggest that the complex and ligand follow an energy-dependent pathway of cellular uptake (Figure 4b). Further, even after a prolonged incubation of the complex and ligand for 4 h, no increase in emission intensity was found in the treated cells incubated at 4 °C (Figure S14 in the Supporting Information).

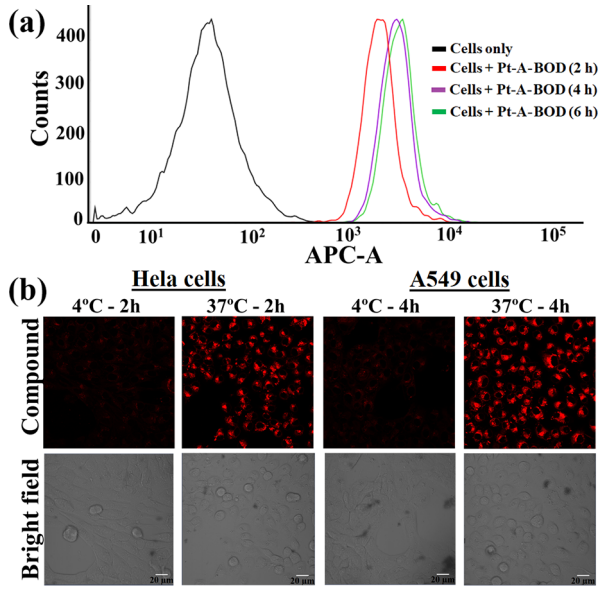


**Figure 4.** (a) Quantitative analysis of cellular uptake of the compounds by flow cytometry upon incubating A549 cells with **Pt-A-BOD** (2 $\mu$M) at 37 °C at different time intervals along with untreated cells used as a control. (b) Confocal images of HeLa (left panels) and A549 (right panels) cells incubated with **Pt-A-BOD** (2 $\mu$M) at two different temperatures, namely 37 and 4 °C, for 4 h. Scale bar: 20 $\mu$m.

The red fluorescence emission property at 720 nm from the complex **Pt-A-BOD** in 1% DMSO/DMEM enabled us to carry out real-time imaging in live cells. This property is useful to understand the cellular uptake mechanism of a drug in live cells by recording pictures constantly at different time intervals or at no time intervals. The cellular entry of the complex **Pt-A-BOD** (1 $\mu$M) in 1% DMSO/DMEM was visualized in A549 cells through live cell imaging by maintaining a 5% $CO_2$ atmosphere at 37 °C. Images were recorded immediately after treatment with the complex **Pt-A-BOD** (1 $\mu$M) with no time interval and a band path of 660−750 nm by using $\lambda_{ex}$ = 633 nm. The entry of the complex was observed within 100 s of incubation from fluorescence emission and complete localization, and the maximum uptake was reached 750 s after the treatment. Further, the cells did not show any major increase in fluorescence or varied localization (Figure S15 in the Supporting Information). The CLSM images also indicated punctate fluorescence, suggesting that the uptake pathway is possibly through endocytosis. The results indicated a rapid cellular uptake of the BODIPY complex in A549 cells, suggesting a high cell membrane permeability of the complex.

**Singlet Oxygen as a Cytotoxic Agent.** The objective of appending a monostyryl BODIPY moiety on $\{Pt(NH_3)_2\}^{2+}$ coordinated to a O,O-donor ligand was to generate reactive oxygen species (ROS) on red-light irradiation. The complex

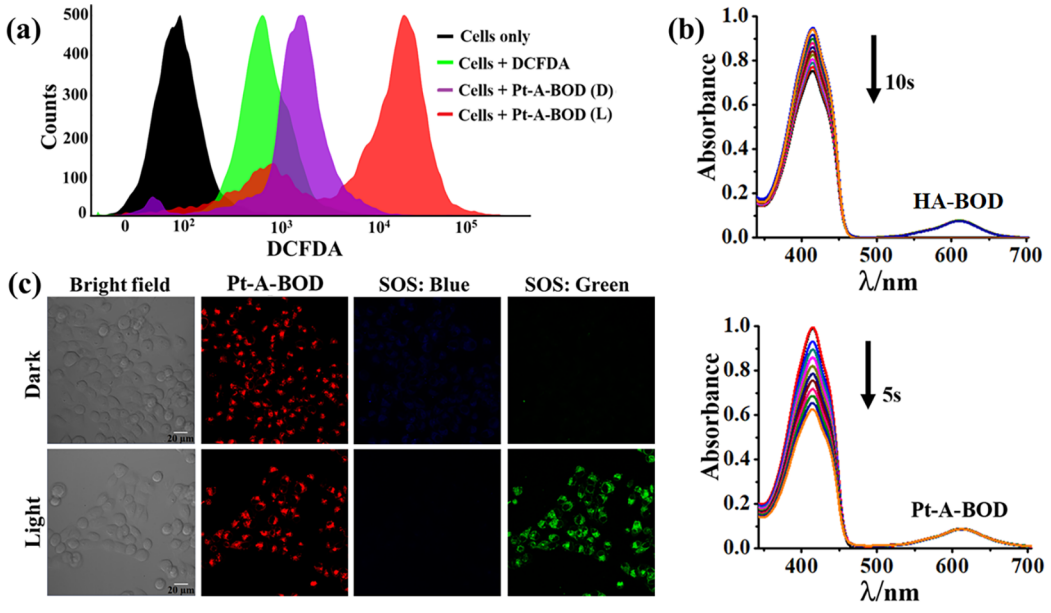


**Figure 5.** (a) Cellular ROS generation by a DCFDA assay in **Pt-A-BOD** (2 $\mu$M, 4 h)-treated A549 cells under red light of 600−720 nm (L, light dose 30 $J$ cm$^{-2}$) and in the dark (D). (b) Spectral variations of DPBF at 417 nm on treatment with the ligand **HA-BOD** and the complex **Pt-A-BOD** in DMF at 5 s intervals under red light irradiation ($\lambda$ = 600−720 nm). (c) Cellular detection of $^1O_2$ generated by **Pt-A-BOD** (2 $\mu$M, 4h) in A549 cells in red light of 600−720 nm (light dose 30 $J$ cm$^{-2}$) and in the dark by an SOS analysis kit (SOS is a singlet oxygen sensor).


https://doi.org/10.1021/acs.inorgchem.1c00124
Inorg. Chem. 2021, 60, 6410−6420

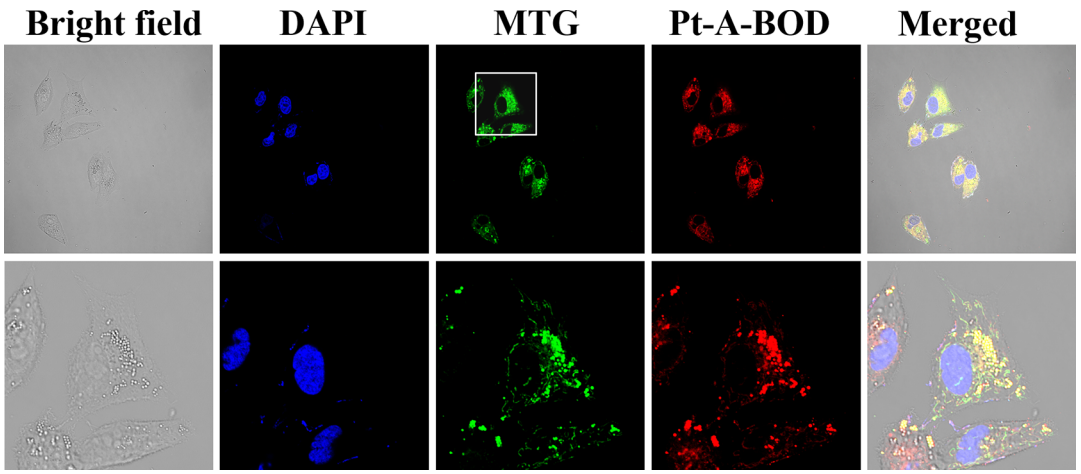


**Figure 6.** Confocal images of A549 cells incubated with red-emitting **Pt-A-BOD** (2 $\mu$M) for 4 h at 37 °C along with Mito Tracker Green (MTG). DAPI (4′,6-diamidino-2-phenylindole) was used as a blue -emitting nuclear staining dye. Scale bar: 20 $\mu$m. Lower panels are the expanded region of the highlighted portion (see box) of the top panels.

**Pt-A-BOD** and ligand H**A-BOD** were developed as novel NIR-PDT photosensitizers for therapeutic applications. To determine the formation of any reactive oxygen species under red-light photoirradiation (600−720 nm) in a cellular environment, a DCFDA (2′,7′-dichlorofluorescein diacetate) assay in A549 cells was carried out. DCFDA is a non-fluorescent compound that has the ability to penetrate the cell membrane and react with any ROS to form green fluorescent 2′,7′-dichlorodihydrofluorescein with a $\lambda_{em}$ value of 525 nm ($\lambda_{ex}$ = 488 nm) upon oxidation. Hence, any generation of ROS can be determined using a flow cytometry analysis by measuring the green fluorescence of 2′,7′-DCF in the FL-1 channel, which would indicate the cell population generating ROS. Two sets of A549 cells were treated with the complex **Pt-A-BOD** and the ligand H**A-BOD** at their $IC_{50}$ concentrations (**Pt-A-BOD**, 2 $\mu$M; H**A-BOD**, 40 $\mu$M) for 4 h followed by irradiation with red light ($\lambda$ = 600−720 nm, light dose 30 $J$ $cm^{-2}$) for one set and samples kept in the dark for the other set. Both sets of cells were further incubated with DCFDA (1 $\mu$M, 10 min) and subjected to a FACS analysis. The cells treated with only DCFDA and the cells treated with the complex **Pt-A-BOD** but kept in the dark showed only a small shift in the histogram. In contrast, **Pt-A-BOD**-treated cells on irradiation with red light displayed a large shift in fluorescence, indicating the ability of **Pt-A-BOD** to generate cytotoxic reactive oxygen species (Figure 5a). A similar observation was made for the cells treated with H**A-BOD** at its $IC_{50}$ concentration (Figure S16 in the Supporting Information). BODIPY dyes as photosensitizers are well-known to generate singlet oxygen as the ROS upon photoexcitation via a type II process in which the photosensitizer in its triplet state transfers energy to triplet oxygen to generate singlet oxygen. To ascertain the nature of ROS generated from **Pt-A-BOD** and H**A-BOD** in red light, a 1,3-diphenylisobenzofuran (DPBF) assay was done in DMF. The absorption spectral intensity of DPBF as a singlet oxygen scavenger in DMF in the presence of the complex and ligand at 417 nm was examined by employing a 660 nm continuous-wave diode laser as the excitation source. At intervals of 5 s, a gradual decrease in the absorbance of DPBF treated with the complex **Pt-A-BOD** at 417 nm was observed in the UV−visible spectral assay. A similar experiment with the ligand H**A-BOD** with 10 s intervals of light irradiation did not show any significant changes. The results indicate much a higher efficacy of singlet oxygen generation by the complex in comparison to the ligand (Figure 5b and Figure S16 in the Supporting Information). The singlet oxygen generation ability of the complex **Pt-A-BOD** inside the cellular medium was determined in A549 cells using a singlet oxygen specific dye: namely, singlet oxygen sensor green (SOSG). SOSG is a dye that displays weak blue fluorescence inside the cellular medium, but in the presence of singlet oxygen the fluorescence emission shifts from blue to green ($\lambda_{em}$ = 525 nm, $\lambda_{ex}$ = 488 nm). Two sets of A549 cells were incubated with the complex **Pt-A-BOD** (2 $\mu$M) for 4 h followed by treatment with SOSG dye (100 $\mu$M) for 20 min. After the removal of the buffer containing SOSG, one set of cells was subjected to irradiation using red light ($\lambda$ = 600−720 nm, light dose 30 $J$ $cm^{-2}$), while the other set was kept in the dark. The cells were subjected to CLSM. The complex-treated cells without red light irradiation displayed a weak blue fluorescence inside the cells, but no fluorescence was observed in the green region (Figure 5c). In contrast, the cells treated with the complex and irradiated under red light ($\lambda$ = 600−720 nm, light dose = 30 $J$ $cm^{-2}$) displayed bright green fluorescence in the green channel but no blue fluorescence. The results unequivocally showed the cellular generation of singlet oxygen by the complex **Pt-A-BOD** in red light.

**Mitochondrial Localization.** The appended BODIPY moiety enabled us to employ complex **Pt-A-BOD** for cellular imaging as a NIR fluorophore that would inhibit the intervention of background signals occurring due to tissue autofluorescence. To determine the target organelle of the complex (2 $\mu$M), A549 cells were incubated for 2 h at 37 °C in the dark and were later subjected to confocal laser scanning microscopy. The cells retained good morphology after 24 h of incubation, and the CLSM images of the complex-incubated cells were captured with a band path of 650−750 nm upon excitation at 633 nm. A study on the localization of the compounds using their fluorescence along with trackers, namely Mito Tracker Green (MTG) and the nucleus-specific dye 4′,6-diamidino-2-phenylindole (DAPI), was carried out for A549 cells. The CLSM merged images of the complex and DAPI clearly indicated its localization in the cytoplasm rather than the nucleus. The red fluorescence emission caused by the


https://doi.org/10.1021/acs.inorgchem.1c00124
Inorg. Chem. 2021, 60, 6410−6420

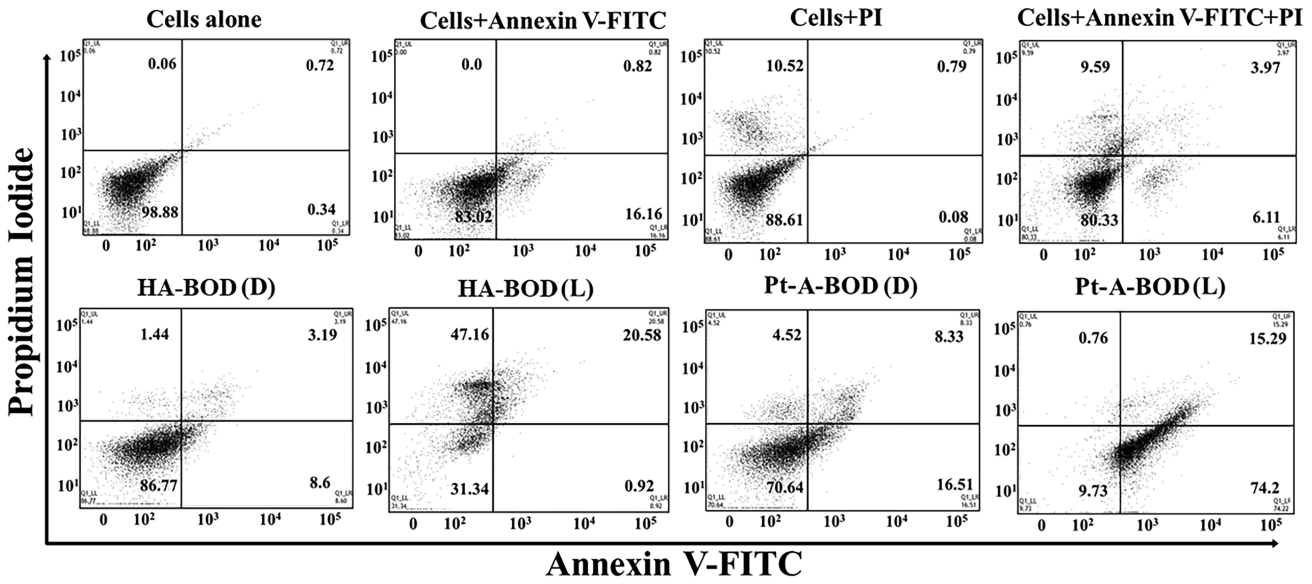


**Figure 7.** AnnexinV-FITC and propidium iodide (PI) staining of A549 cells that undergo apoptosis/necrosis caused by the compounds **Pt-A-BOD** (2 $\mu$M) and H**A-BOD** (40 $\mu$M) in red light of 600−720 nm (L, light dose 30 $J$ cm$^{-2}$) and in the dark (D) by FACS analysis. The percent cell population can be viewed in the respective quadrants: lower left for live cells, lower right for early apoptotic cells, upper right for late apoptotic cells, and upper left for dead cells.

complex merged with the green fluorescence of MTG, showing a strong overlapping with an overlap coefficient value of 93%. This indicated significant localization of the complex in the mitochondria of A549 lung cancer cells (Figure 6 and Figure S17 in the Supporting Information). Similar results were obtained with the merged images of the ligand H**A-BOD** and the trackers MTG and DAPI, with a clear indication that the complex **Pt-A-BOD** is localized in the mitochondria due to the presence of the coordinated ligand **A-BOD** (Figure S18 inthe Supporting Information). The mitochondrial localization achieved by both the ligand and the complex can be attributed as well to the presence of *N*,*N*-dimethylaniline as a monostyryl unit in the BODIPY ligand H**A-BOD**. For a fluorophore to be employed for cellular imaging, the bleaching of the dye should be at a minimum with negligible effects on the cellular morphology. A549 cells were incubated with the complex **Pt-A-BOD** (2 $\mu$M) for 2 h and then subjected to CLSM. A frame of the red fluorescence image of the complex was fixed, images were recorded constantly at time intervals of 1 min for a period of 20 min. With no signs of morphological changes in the cells, we observed a minor decrease in the fluorescence intensity from the first recorded image to the last image, clearly indicating negligible bleaching of complex **Pt-A-BOD** as a dye inside the live cellular medium under 5% $CO_2$ at 37 °C (Figure S19 in the Supporting Information). This property of the complex can be effectively employed for the intracellular imaging and tracking of a drug to gain complete insight into the mechanism of drug action.

**Cellular Apoptosis.** The cellular death pathway induced by the complex **Pt-A-BOD** and the ligand H**A-BOD** under red-light photoirradiation was determined by an AannexinV-FITC/PI assay in A549 cells. Two sets of A549 cells were treated with the complex (2 $\mu$M) and the ligand (40 $\mu$M) at their $IC_{50}$ values and incubated for 4 h in the dark. One set of cells after removal of the compounds was kept in the dark (D), while the other set of cells was irradiated with red light of 600−720 nm (L, light dose 30 $J$ cm$^{-2}$). With the untreated cells, the FITC fluorescence and PI fluorescence were stabilized to a minimum level. The results showed that ∼74% of the cells in the **Pt-A-BOD**-treated set of cells in light (L) were in an early apoptotic phase and ∼15% of the cells were in a late apoptotic phase with no cells being found to have a necrotic death pathway (Figure 7). For the **Pt-A-BOD**-treated set of cells in the dark (D), ∼17% of the cells were in an early apoptotic phase, while ∼8.3% of the cells were in the late apoptosis phase and ∼4% cells in the necrotic death pathway. In contrast, for H**A-BOD**-treated set of cells in the light (L), ∼1% of the cells were in an early apoptosis phase, ∼21% of the cells were in a late apoptotic phase, and remarkably ∼47% of the cells were in a necrotic death pathway (Figure 7). There was not much change in the results of the ligand **HA-BOD**-treated set of cells in the dark (D) in comparison to the set of cells that were untreated. The results clearly suggest apoptotic cellular death induced by complex **Pt-A-BOD** in light, while the pathway is predominantly necrotic for the ligand H**A-BOD**.

**Mitochondrial Membrane Potential.** Complex **Pt-A-BOD** in A549 cells induced an apoptotic pathway of cell death on irradiation with red light. The confocal imaging results indicated specific mitochondrial localization. To further determine the possible damage that would occur in the mitochondria of A549 cells treated with this complex, a JC1 assay was performed to study the mitochondrial membrane integrity. Two sets of A549 cells were treated with the complex (2 $\mu$M) at its $IC_{50}$ value and incubated for 4 h in the dark. One set of the cells after removal of the complex was kept in the dark (D), while the other set of cells was irradiated with red light of 600−720 nm (L, light dose 30 $J$ cm$^{-2}$). JC1 dye is known to show red fluorescence inside the cells when the mitochondrial membrane potential remains intact. The dye, however, displays green fluorescence when the mitochondrial membrane potential is altered. The complex-treated set of cells in the light (L) exhibited bright green fluorescence of the JC1 dye with negligible red fluorescence (Figure 8). However, the complex-treated set of cells kept in the dark (D) showed red fluorescence of the JC1 dye with negligible green fluorescence,


https://doi.org/10.1021/acs.inorgchem.1c00124
*Inorg. Chem.* 2021, 60, 6410−6420

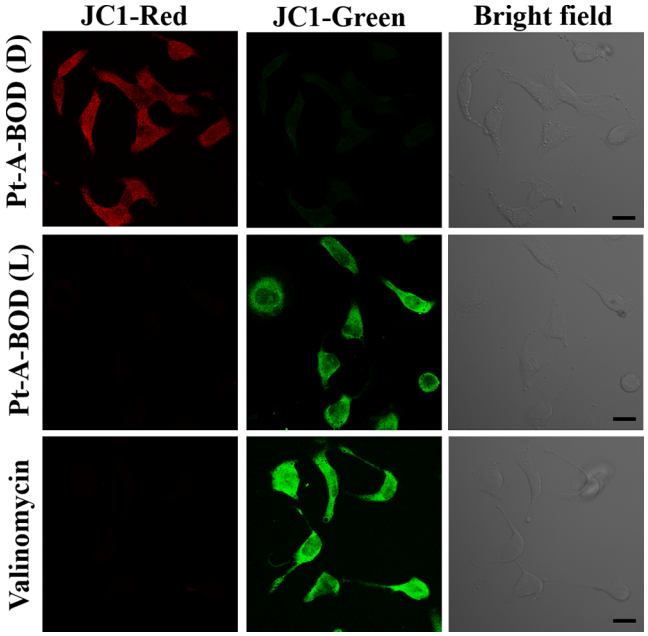


**Figure 8.** Confocal microscopic images of the JC-1 assay showing the fluorescence images of JC-1 dye in both red and green channels in A549 cells incubated with the complex **Pt-A-BOD** (2 $\mu$M) for 4 h at 37 °C in the dark and on red-light photoirradiation ($\lambda$ = 600−720 nm; light dose 30 $J$ cm$^{-2}$). The scale bar is 20 $\mu$m in all of the panels.

clearly indicating that the complex did not alter the mitochondrial membrane potential in the dark but altered it on irradiation with red light.

## CONCLUSIONS

A platinum(II) complex, [Pt(**A-BOD**)$(NH_3)_2$]$(NO_3)$ (**Pt-A-BOD**, Maloplatin-B), as a cisplatin analogue having monoanionic *O,O*-donor methyl malonyl moiety-conjugated to monostyryl BODIPY ligand (H**A-BOD**) was designed, synthesized, and exemplified as an efficient near-IR red-light-active photodynamic therapy (PDT) agent against cancer cells, while it is dormant against immortalized human lung epithelial cells. The non-BODIPY complex [Pt(acac)$(NH_3)_2$]$(NO_3)$ (**Pt-Ac**) was used as a control, which showed no significant activity in the dark or light. The complex **Pt-A-BOD** showed rapid cellular uptake in lung cancer A549 cells through an energy-dependent pathway. It predominantly localized in the mitochondria of the cancer cells and produced singlet oxygen ($^1O_2$) as the ROS, targeting this specific organelle under NIR light irradiation (600−720 nm). In HeLa and A549 cancer cells, the BODIPY complex induced remarkable photocytotoxicity in the PDT spectral window of 650−850 nm with $IC_{50}$ values within 1.6−2.4 $\mu$M while being effectively nontoxic in dark. The PDT activity is based on the high-yield generation of singlet oxygen inside the cells on red-light irradiation. The ligand H**A-BOD**, due to its lower singlet oxygen quantum yield and lower cellular uptake in comparison to its complex, gave relatively higher $IC_{50}$ values, thus indicating its reduced photocytotoxicity. The ligand followed a necrotic pathway of cell death, while the complex primarily showed the desirable apoptotic pathway. The complex caused significant changes in the mitochondrial membrane potential, leading to apoptotic cell death in A549 cancer cells. It showed higher stability with lower bleaching properties, thus making it a potential therapeutic agent suitable for dual application: namely, near-IR-light cellular imaging and PDT activity. This work exemplifies a rare cisplatin analogue having monostyryl BODIPY as a near-IR-light PDT agent localizing in mitochondria and causing cellular apoptosis on singlet oxygen generation.

## ASSOCIATED CONTENT

### Supporting Information

The Supporting Information is available free of charge at https://pubs.acs.org/doi/10.1021/acs.inorgchem.1c00124.

Reaction schemes, ESI-mass, NMR, and IR spectra, stability plots, MTT assay, cellular uptake, DCFDA assay, confocal images, Cartesian coordinates, and bond distances/angles of the ligand H**A-BOD** and complex **Pt-A-BOD** (PDF)

## AUTHOR INFORMATION

### Corresponding Authors

**Paturu Kondaiah** − *Department of Molecular Reproduction, Development and Genetics, Indian Institute of Science, Bangalore 560012, India*; Phone: +91-80-22932688; Email: paturu@iisc.ac.in; Fax: +91-80-23600999

**Akhil R. Chakravarty** − *Department of Inorganic and Physical Chemistry, Indian Institute of Science, Bangalore 560012, India*; orcid.org/0000-0002-6471-9167; Phone: +91-80-22932533; Email: arc@iisc.ac.in; Fax: +91-80-23600683

### Authors

**Vanitha Ramu** − *Department of Inorganic and Physical Chemistry, Indian Institute of Science, Bangalore 560012, India*; orcid.org/0000-0003-4438-1071

**Paramita Kundu** − *Department of Molecular Reproduction, Development and Genetics, Indian Institute of Science, Bangalore 560012, India*; orcid.org/0000-0003-4538-4573

Complete contact information is available at: https://pubs.acs.org/10.1021/acs.inorgchem.1c00124

### Notes

The authors declare no competing financial interest.

## ACKNOWLEDGMENTS

A.R.C. thanks the Department of Science and Technology (DST), Government of India, New Delhi, for financial support (SR/S5/MBD-02/2007, EMR/2015/000742, CRG/2018/000081) and for a J. C. Bose national fellowship (SR/S2/JCB-26/2007). P.K.'s research group is funded by DBT-IISc grants. We are grateful to Ms. Leepika for help in recording FACS data and Ms. Saima and Ms. Divya for help in acquiring confocal microscopic images from the Division of Biological Sciences, IISc Bangalore.

## REFERENCES

(1) Alderden, R. A.; Hall, M. D.; Hambley, T. W. The Discovery and Development of Cisplatin. *J. Chem. Educ.* **2006**, *83*, 728−734.

(2) Wilson, J. J.; Lippard, S. J. Synthetic Methods for the Preparation of Platinum Anticancer Complexes. *Chem. Rev.* **2014**, *114*, 4470−4495.

(3) Lebwohl, D.; Canetta, R. Clinical Development of Platinum Complexes in Cancer Therapy: An Historical Perspective and an Update. *Eur. J. Cancer* **1998**, *34*, 1522−1534.

(4) Wang, X.; Wang, X.; Guo, Z. Functionalization of Platinum Complexes for Biomedical Applications. *Acc. Chem. Res.* **2015**, *48*, 2622−2631.
(5) Johnstone, T. C.; Suntharalingam, K.; Lippard, S. J. The Next Generation of Platinum Drugs: Targeted Pt(II) Agents, Nanoparticle Delivery, and Pt(IV) Prodrugs. *Chem. Rev.* **2016**, *116*, 3436−3486.
(6) Kelland, L. The Resurgence of Platinum-Based Cancer Chemotherapy. *Nat. Rev. Cancer* **2007**, *7*, 573−584.
(7) Alcindor, T.; Beauger, N. Oxaliplatin: A Review in the Era of Molecularly Targeted Therapy. *Curr. Oncol.* **2011**, *18*, 18−25.
(8) Pavelka, M.; Lucas, M. F. A.; Russo, N. On the Hydrolysis Mechanism of the Second-Generation Anticancer Drug Carboplatin. *Chem. - Eur. J.* **2007**, *13*, 10108−10116.
(9) (a) Ndagi, U.; Mhlongo, N.; Soliman, M. E. Metal Complexes in Cancer Therapy − an Update from Drug Design Perspective. *Drug Des., Dev. Ther.* **2017**, *11*, 599−616. (b) Farrell, N. P. Multi-Platinum Anti-Cancer Agents. Substitution-Inert Compounds for Tumor Selectivity and New Targets. *Chem. Soc. Rev.* **2015**, *44*, 8773−8785.
(10) Choi, C. H.; Cha, Y. J.; An, C. S.; Kim, K. J.; Kim, K. C.; Moon, S. P.; Lee, Z. H.; Min, Y. D. Molecular Mechanisms of Heptaplatin Effective against Cisplatin-Resistant Cancer Cell Lines: Less Involvement of Metallothfionein. *Cancer Cell Int.* **2004**, *4*, 6.
(11) Zhou, J.; Kang, Y.; Chen, L.; Wang, H.; Liu, J.; Zeng, S.; Yu, L. The Drug-Resistance Mechanisms of Five Platinum-Based Antitumor Agents. *Front. Pharmacol.* **2020**, *11*, 1−17.
(12) Shah, N.; Dizon, D. S. New-Generation Platinum Agents for Solid Tumors. *Future Oncol.* **2009**, *5*, 33−42.
(13) Wheate, N. J.; Walker, S.; Craig, G. E.; Oun, R. The Status of Platinum Anticancer Drugs in the Clinic and in Clinical Trials. *Dalton Trans.* **2010**, *39*, 8113−8127.
(14) Zhong, L. Z.; Xu, H. Y.; Zhao, Z. M.; Zhang, G. M.; Lin, F. W. Comparison of Efficacy and Toxicity between Nedaplatin and Cisplatin in Treating Malignant Pleural Effusion. *OncoTargets Ther.* **2018**, *11*, 5509−5512.
(15) (a) Imran, M.; Ayub, W.; Butler, I. S.; Zia-Ur-Rehman. Photoactivated Platinum-Based Anticancer Drugs. *Coord. Chem. Rev.* **2018**, *376*, 405−429. (b) Imran, M.; Zia-Ur-Rehman; Kondratyuk, T.; Belanger-Gariepy, F. New Ternary Platinum(II) Dithiocarbamates: Synthesis, Characterization, Anticancer, DNA Binding and DNA Denaturing Studies. *Inorg. Chem. Commun.* **2019**, *103*, 12−20. (c) Kashif Amir, M.; Hogarth, G.; Khan, Z.; Imran, M.; Zia-ur-Rehman. *Inorg. Chim. Acta* **2020**, *512*, 119853−119863. (d) Lovejoy, K. S.; Serova, M.; Bieche, I.; Emami, S.; D'Incalci, M.; Broggini, M.; Erba, E.; Gespach, C.; Cvitkovic, E.; Faivre, S.; Raymond, E.; Lippard, S. J. Anticancer Activity of Pyriplatin, A Monofunctional Cationic Platinum(II) Compound, in Human Cancer Cells. *Mol. Cancer Ther.* **2011**, *10*, 1709−1719.
(16) Park, G. Y.; Wilson, J. J.; Song, Y.; Lippard, S. J. Phenanthriplatin, a Monofunctional DNA-Binding Platinum Anticancer Drug Candidate with Unusual Potency and Cellular Activity Profile. *Proc. Natl. Acad. Sci. U. S. A.* **2012**, *109*, 11987−11992.
(17) (a) Hall, M. D.; Mellor, H. R.; Callaghan, R.; Hambley, T. W. Basis for design and development of platinum(IV) anticancer complexes. *J. Med. Chem.* **2007**, *50*, 3403−3411. (b) Raynaud, F. I.; Boxall, F. E.; Goddard, P.; Barnard, C. F.; Murrer, B. A.; Kelland, L. R. Metabolism, Protein Binding and In Vivo Activity of the Oral Platinum Drug JM216 and its Biotransformation Products. *Anticancer Res.* **1996**, *16*, 1857−1862. (c) Gibson, D. Platinum(IV) Anticancer Prodrugs-Hypotheses and Facts. *Dalton Trans.* **2016**, *45*, 12983−12991. (d) Guo, Z.; Sadler, P. J. Metals in Medicine. *Angew. Chem., Int. Ed.* **1999**, *38*, 1512−1531.
(18) (a) Chin, C. F.; Wong, D. Y. Q.; Jothibasu, R.; Ang, W. H. Anticancer platinum(IV) prodrugs with novel modes of activity. *Curr. Top. Med. Chem.* **2011**, *11*, 2602−2612. (b) Ma, J.; Wang, Q.; Huang, Z.; Yang, X.; Nie, Q.; Hao, W.; Wang, P. G.; Wang, X. Glycosylated Platinum(IV) Complexes as Substrates for Glucose Transporters (GLUTs) and Organic Cation Transporters (OCTs) Exhibited Cancer Targeting and Human Serum Albumin Binding Properties for Drug Delivery. *J. Med. Chem.* **2017**, *60*, 5736−5748.
(19) Zhao, J.; Hua, W.; Xu, G.; Gou, S. Biotinylated Platinum(IV) Complexes Designed to Target Cancer Cells. *J. Inorg. Biochem.* **2017**, *176*, 175−180.
(20) Bonnet, S. Why Develop Photoactivated Chemotherapy? *Dalton Trans.* **2018**, *47*, 10330−10343.
(21) Farrer, N. J.; Salassa, L.; Sadler, P. J. Photoactivated Chemotherapy (PACT): The Potential of Excited-State d-Block Metals in Medicine. *Dalton Trans.* **2009**, *44*, 10690−10701.
(22) Shi, H.; Imberti, C.; Sadler, P. J. Diazido Platinum(IV) Complexes for Photoactivated Anticancer Chemotherapy. *Inorg. Chem. Front.* **2019**, *6*, 1623−1638.
(23) Dąbrowski, J. M.; Arnaut, L. G. Photodynamic Therapy (PDT) of Cancer: From Local to Systemic Treatment. *Photochem. Photobiol. Sci.* **2015**, *14*, 1765−1780.
(24) Castano, A. P.; Mroz, P.; Hamblin, M. R. Photodynamic Therapy and Anti-Tumour Immunity. *Nat. Rev. Cancer* **2006**, *6*, 535−545.
(25) Doherty, R. E.; Sazanovich, I. V.; McKenzie, L. K.; Stasheuski, A. S.; Coyle, R.; Baggaley, E.; Bottomley, S.; Weinstein, J. A.; Bryant, H. E. Photodynamic Killing of Cancer Cells by a Platinum(II) Complex with Cyclometallating Ligand. *Sci. Rep.* **2016**, *6*, 1−9.
(26) Raza, M. K.; Gautam, S.; Howlader, P.; Bhattacharyya, A.; Kondaiah, P.; Chakravarty, A. R. Pyriplatin-Boron-Dipyrromethene Conjugates for Imaging and Mitochondria-Targeted Photodynamic Therapy. *Inorg. Chem.* **2018**, *57*, 14374−14385.
(27) Heinemann, F.; Karges, J.; Gasser, G. Critical Overview of the Use of Ru(II) Polypyridyl Complexes as Photosensitizers in One-Photon and Two-Photon Photodynamic Therapy. *Acc. Chem. Res.* **2017**, *50*, 2727−2736.
(28) Mao, J.; Zhang, Y.; Zhu, J.; Zhang, C.; Guo, Z. Molecular Combo of Photodynamic Therapeutic Agent Silicon(Iv) Phthalocyanine and Anticancer Drug Cisplatin. *Chem. Commun.* **2009**, *8*, 908−910.
(29) (a) Mitra, K.; Lyons, C. E.; Hartman, M. C. T. A Platinum(II) Complex of Heptamethine Cyanine for Photoenhanced Cytotoxicity and Cellular Imaging in Near-IR Light. *Angew. Chem., Int. Ed.* **2018**, *57*, 10263−10267. (b) Naik, A.; Rubbiani, R.; Gasser, G.; Spingler, B. Visible-Light-Induced Annihilation of Tumor Cells with Platinum-Porphyrin Conjugates. *Angew. Chem., Int. Ed.* **2014**, *53*, 6938−6941.
(30) Raza, M. K.; Gautam, S.; Garai, A.; Mitra, K.; Kondaiah, P.; Chakravarty, A. R. Monofunctional BODIPY-Appended Imidazoplatin for Cellular Imaging and Mitochondria-Targeted Photocytotoxicity. *Inorg. Chem.* **2017**, *56*, 11019−11029.
(31) Kou, J.; Dou, D.; Yang, L. Porphyrin Photosensitizers in Photodynamic Therapy and Its Applications. *Oncotarget* **2017**, *8*, 81591−81603.
(32) Ethirajan, M.; Chen, Y.; Joshi, P.; Pandey, R. K. The Role of Porphyrin Chemistry in Tumor Imaging and Photodynamic Therapy. *Chem. Soc. Rev.* **2011**, *40*, 340−362.
(33) Sharman, W. M.; Allen, C. M.; Van Lier, J. E. Photodynamic Therapeutics: Basic Principles and Clinical Applications. *Drug Discovery Today* **1999**, *4*, 507−517.
(34) Zhu, S.; Yao, S.; Wu, F.; Jiang, L.; Wong, K. L.; Zhou, J.; Wang, K. Platinated Porphyrin as a New Organelle and Nucleus Dual-Targeted Photosensitizer for Photodynamic Therapy. *Org. Biomol. Chem.* **2017**, *15*, 5764−5771.
(35) Mitra, K.; Gautam, S.; Kondaiah, P.; Chakravarty, A. R. BODIPY-Appended 2-(2-Pyridyl)Benzimidazole Platinum(II) Catecholates for Mitochondria-Targeted Photocytotoxicity. *ChemMedChem* **2016**, *11*, 1956−1967.
(36) Paul, S.; Kundu, P.; Bhattacharyya, U.; Garai, A.; Maji, R. C.; Kondaiah, P.; Chakravarty, A. R. Ruthenium(II) Conjugates of Boron-Dipyrromethene and Biotin for Targeted Photodynamic Therapy in Red Light. *Inorg. Chem.* **2020**, *59*, 913−924.
(37) Ramu, V.; Gautam, S.; Garai, A.; Kondaiah, P.; Chakravarty, A. R. Glucose-Appended Platinum(II)-BODIPY Conjugates for Targeted Photodynamic Therapy in Red Light. *Inorg. Chem.* **2018**, *57*, 1717−1726.


https://doi.org/10.1021/acs.inorgchem.1c00124
*Inorg. Chem.* 2021, 60, 6410−6420

(38) Garai, A.; Gandhi, A.; Ramu, V.; Raza, M. K.; Kondaiah, P.; Chakravarty, A. R. Photochemotherapy of Infrared Active BODIPY-Appended Iron(III) Catecholates for in Vivo Tumor Growth Inhibition. *ACS Omega* **2018**, *3*, 9333−9338.
(39) Bhattacharyya, A.; Dixit, A.; Mitra, K.; Banerjee, S.; Karande, A. A.; Chakravarty, A. R. BODIPY Appended Copper(II) Complexes of Curcumin Showing Mitochondria Targeted Remarkable Photocytotoxicity in Visible Light. *MedChemComm* **2015**, *6*, 846−851.
(40) Mukherjee, N.; Podder, S.; Banerjee, S.; Majumdar, S.; Nandi, D.; Chakravarty, A. R. Targeted Photocytotoxicity by Copper(II) Complexes Having Vitamin B6and Photoactive Acridine Moieties. *Eur. J. Med. Chem.* **2016**, *122*, 497−509.
(41) (a) Liu, Y.; Li, Z.; Chen, L.; Xie, Z. Near Infrared BODIPY-Platinum Conjugates for Imaging, Photodynamic Therapy and Chemotherapy. *Dyes Pigm.* **2017**, *141*, 5−12. (b) Loudet, A.; Burgess, K. BODIPY Dyes and Their Derivatives: Syntheses and Spectroscopic Properties. *Chem. Rev.* **2007**, *107*, 4891−4932.
(42) Chen, K.; Dong, Y.; Zhao, X.; Imran, M.; Tang, G.; Zhao, J.; Liu, Q. Bodipy Derivatives as Triplet Photosensitizers and the Related Intersystem Crossing Mechanisms. *Front. Chem.* **2019**, *7*, 1−14.
(43) Turksoy, A.; Yildiz, D.; Akkaya, E. U. Photosensitization and Controlled Photosensitization with BODIPY Dyes. *Coord. Chem. Rev.* **2019**, *379*, 47−64.
(44) Kowada, T.; Maeda, H.; Kikuchi, K. BODIPY-Based Probes for the Fluorescence Imaging of Biomolecules in Living Cells. *Chem. Soc. Rev.* **2015**, *44*, 4953−4972.
(45) Kue, C. S.; Ng, S. Y.; Voon, S. H.; Kamkaew, A.; Chung, L. Y.; Kiew, L. V.; Lee, H. B. Recent Strategies to Improve Boron Dipyrromethene (BODIPY) for Photodynamic Cancer Therapy: An Updated Review. *Photochem. Photobiol. Sci.* **2018**, *17*, 1691−1708.
(46) Kamkaew, A.; Lim, S. H.; Lee, H. B.; Kiew, L. V.; Chung, L. Y.; Burgess, K. BODIPY Dyes in Photodynamic Therapy. *Chem. Soc. Rev.* **2013**, *42*, 77−88.
(47) Ramu, V.; Gautam, S.; Kondaiah, P.; Chakravarty, A. R. Diplatinum(II) Catecholate of Photoactive Boron-Dipyrromethene for Lysosome-Targeted Photodynamic Therapy in Red Light. *Inorg. Chem.* **2019**, *58*, 9067−9075.
(48) (a) Stacey, O. J.; Ward, B. D.; Coles, S. J.; Horton, P. N.; Pope, S. J. A. Chromophore-Labelled, Luminescent Platinum Complexes: Syntheses, Structures, and Spectroscopic Properties. *Dalton Trans.* **2016**, *45*, 10297−10307. (b) Ünlü, H.; Okutan, E. Preparation of BODIPY- Fullerene and Monostyryl BODIPY-Fullerene Dyads as Heavy Atom Free Singlet Oxygen Generators. *Dyes Pigm.* **2017**, *142*, 340−349.
(49) Mitra, K.; Gautam, S.; Kondaiah, P.; Chakravarty, A. R. The Cis-Diammineplatinum(II) Complex of Curcumin: A Dual Action DNA Crosslinking and Photochemotherapeutic Agent. *Angew. Chem., Int. Ed.* **2015**, *54*, 13989−13993.
(50) Frisch, M. J.; Trucks, G. W.; Schlegel, H. B.; Scuseria, G. E.; Robb, M. A.; Cheeseman, J. R.; Scalmani, G.; Barone, V.; Mennucci, B.; Petersson, G. A.; Nakatsuji, H.; Caricato, M.; Li, H. P.; Hratchian, A. F.; Izmaylov, J.; Bloino, G.; Zheng, J. L.; Sonnenberg, M.; Hada, M. E.; Toyota, K.; Fukuda, R.; Hasegawa, J.; Ishida, M.; Nakajima, T.; Honda, Y.; Kitao, O.; Nakai, H.; Vreven, T.; Montgomery, J. A., Jr.; Peralta, J. E.; Ogliaro, F.; Bearpark, M.; Heyd, J. J.; Brothers, E.; Kudin, K. N.; Staroverov, V. N.; Kobayashi, R.; Normand, J.; Raghavachari, K.; Rendell, A.; Burant, J. C.; Iyengar, S. S.; Tomasi, J.; Cossi, M.; Rega, N.; Millam, J. M.; Klene, M.; Knox, J. E.; Cross, J. B.; Bakken, V.; Adamo, C.; Jaramillo, J.; Gomperts, R.; Stratmann, R. E.; Yazyev, O.; Austin, A. J.; Cammi, R.; Pomelli, C.; Ochterski, J. W.; Martin, R. L.; Morokuma, K.; Zakrzewski, V. G.; Voth, G. A.; Salvador, P.; Dannenberg, J. J.; Dapprich, S.; Daniels, A. D.; Farkas, Ö.; Foresman, J. B.; Ortiz, J. V.; Cioslowski, J.; Fox, D. J. *Gaussian 09, Rev. A.1*; Gaussian, Inc.: Wallingford, CT, 2009.
(51) (a) Becke, A. D. Density-Functional Exchange-Energy Approximation with Correct Asymptotic Behavior. *Phys. Rev. A: At., Mol., Opt. Phys.* **1988**, *38*, 3098−3100. (b) Becke, A. D. Density-Functional Thermochemistry. III. The Role of Exact Exchange. *J. Chem. Phys.* **1993**, *98*, 5648.
(52) (a) Paitandi, R. P.; Mukhopadhyay, S.; Singh, R. S.; Sharma, V.; Mobin, S. M.; Pandey, D. S. Anticancer Activity of Iridium(III) Complexes Based on a Pyrazole-Appended Quinoline-Based BODIPY. *Inorg. Chem.* **2017**, *56*, 12232−12247. (b) Amir, M. K.; Khan, S. Z.; Hayat, F.; Hassan, A.; Butler, I. S.; Zia-Ur-Rehman. Anticancer Activity, DNA-Binding and DNA-Denaturing Aptitude of Palladium(II) Dithiocarbamates. *Inorg. Chim. Acta* **2016**, *451*, 31−40.


https://doi.org/10.1021/acs.inorgchem.1c00124
*Inorg. Chem.* 2021, 60, 6410−6420